Potential-Scanning Localized Surface Plasmon Resonance Sensor

Hiroyasu Nishi, Sayaka Hiroya, and Tetsu Tatsuma*

Institute of Industrial Science, The University of Tokyo, 4-6-1 Komaba, Meguro-ku, Tokyo 153-8505, Japan

ABSTRACT Localized surface plasmon resonance (LSPR) sensors based on plasmonic nanoparticles attract much attention recently. Here we propose a new class of LSPR sensor, that is, a potential-scanning LSPR sensor, in which electron density of the plasmonic nanoparticles is controlled by potential scanning. The sensor exhibits a resonance peak during the potential scan, which negatively shifts with increasing local refractive index. Therefore, the present sensor can be applied to affinity biosensors and chemical sensors based on potential scan instead of wavelength scan. The potential-scanning LSPR sensors do not require space and a mechanical device for wavelength scanning, so the sensors are advantageous for miniaturization and cost reduction, in comparison with the conventional LSPR sensors. We explain the principle and theoretical sensitivities of the potential-scanning LSPR sensors, and refractometry is demonstrated using a sensor with an ITO electrode loaded with gold nanospheres (13 or 40 nm diameter) or nanorods. The smaller and larger nanospheres are suitable for sensing with a wider dynamic range and with a higher sensitivity, respectively. The use of nanorods further improves the sensitivity and figure of merit.

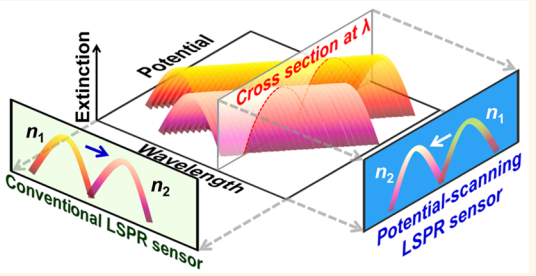

KEYWORDS: LSPR sensor · gold nanoparticle · single-wavelength measurements · potential scanning · refractive index

Detection of molecular interactions is of great importance for chemical, medical, environmental, and food analyses. Localized surface plasmon resonance (LSPR) sensors have been widely utilized to detect such interactions with high sensitivity. Plasmonic metal nanoparticles absorb and scatter light on the basis of LSPR, and the plasmonic extinction (absorption + scattering) peak is red-shifted with increasing local refractive index[1−4] or decreasing interparticle distance.[2,3,5,6] Thus, if a plasmonic nanoparticle is modified with a receptor (*e.g.*, antibody) that binds specifically to a target analyte (*e.g.*, antigen), binding of the analyte to the receptor increases the local refractive index around the particle[1−4] or decreases the interparticle distance,[2,3,6] resulting in a red shift of the plasmonic extinction peak. The analyte concentration or the binding behavior can be monitored on the basis of the spectral peak (or dip[7]) shifts. The LSPR sensors are frequently used for affinity-based chemical sensing and biosensing.[1−4,6,8,9]

Although sensitivity of an LSPR sensor is often lower than that of a propagating surface plasmon resonance (SPR) sensor,[8−11] the former has more localized sensing volume than the latter[4,8] and the sensitivity of the former is being improved further.[4,9] In addition, LSPR sensing can be performed on the basis of a simple extinction measurement without precise control of incident angle and temperature.[4] For an LSPR sensor, however, a monochromator is necessary to obtain spectral peaks, so that a grating must be scanned mechanically or a multichannel photodetector is required. This issue limits the cost and size reduction of the sensor. Although a simple monitoring of extinction at a single wavelength is often performed to address this issue, the single-wavelength method is less accurate because much less information is acquired.

In this study, we propose potential-scanning LSPR sensors as a new class of LSPR sensors that can measure refractive index changes on the basis of resonance peak shifts detected by potential scan instead of wavelength scan. It would only require a small semiconductor laser or a light-emitting diode (LED) with a band-pass filter and an electronic circuit for potential scanning. Here we explain the principle of the potential-scanning LSPR sensing and demonstrate that the sensing is possible with a reasonable resolution of refractive index even by the

* Address correspondence to tatsuma@iis.u-tokyo.ac.jp.

Received for review March 12, 2015 and accepted June 1, 2015.

Published online June 01, 2015
10.1021/acsnano.5b01577

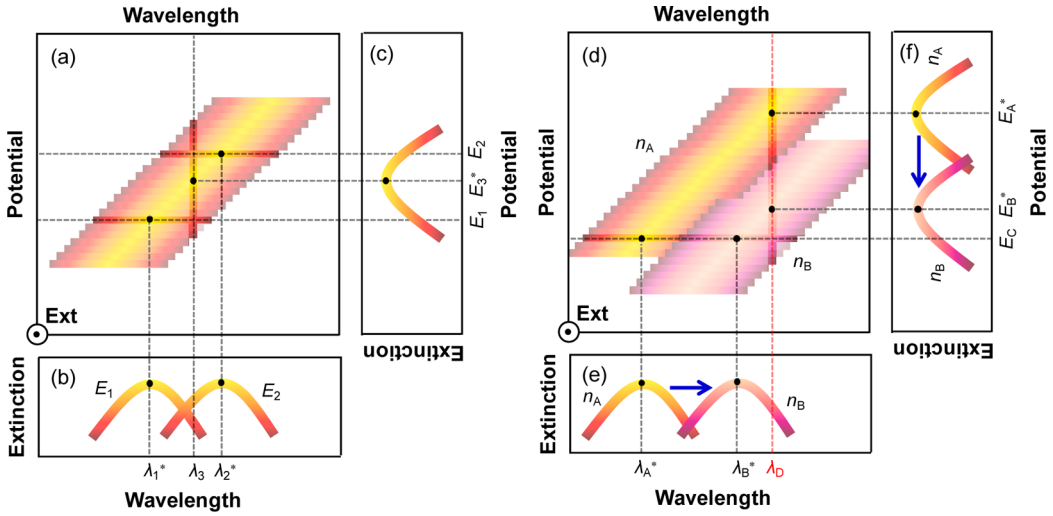

Figure 1. (a) Schematic illustration for a relationship between wavelength (λ), applied potential (E), and extinction (ext) for a plasmonic nanoparticle. (b) Cross sections of panel a at E_1 and E_2 and (c) that at λ_3. (d–f) Plots corresponding to panels a–c at refractive index n_A and n_B. Ext axis is vertical to the sheet in panels a and d.

use of easily or commercially available spherical nanoparticles with a moderate refractive index sensitivity. We also show that the sensitivity can be improved by using nanorods. The present single-wavelength sensor gives much more information than the conventional single-wavelength method. In addition, the present potential-scanning sensor is more suitable for multichannel sensing with miniaturized sensors than the conventional wavelength-scanning sensor. A photosensor array, which is used to obtain an optical spectrum of a wavelength-scanning sensor, can be used for multichannel sensing in the potential-scanning sensor, in which each photosensor pixel is used for each LSPR sensor channel.

RESULTS AND DISCUSSION

Principle of the Potential-Scanning LSPR Sensor. Optical properties of a plasmonic nanoparticle are dependent on applied potential (E).[12−17] A positive shift of E decreases the free electron density of the nanoparticle, resulting in a red shift of its extinction peak. Figure 1a shows a schematic relationship between wavelength (λ), E, and extinction (λ–E–ext plot) for a plasmonic nanoparticle, where the extinction axis is vertical to the sheet. The two curves in Figure 1b (λ–ext plot) are cross-sectional images of Figure 1a at E_1 and E_2. It is clear that a positive potential shift from E_1 to E_2 gives rise to a peak shift from λ_1^* to λ_2^*. On the other hand, Figure 1c (E–ext plot) shows the orthogonal cross section at λ_3, which is peaked at E_3^*. Thus, we can obtain a resonance peak by a potetnial scan at a constant λ.

The optical properties of the plasmonic nanoparticles are well-known to depend also on the refractive index of the surrounding medium (n) as described above: the peak in the λ–ext plot is red-shifted with increasing refractive index. The plots in Figure 1e represent cross sections of the λ–E–ext plots in Figure 1d at E_C. The figure shows that a refractive index increase from n_A to n_B causes a peak shift from λ_A^* to λ_B^*. Meanwhile, cutting the λ–E–ext plots at λ_D gives Figure 1f, in which the peak potential is shifted negatively from E_A^* to E_B^* by the increase of the refractive index from n_A to n_B. It is obvious that the negative potential shift $-(E_B^* - E_A^*)$ is enhanced by an increase in the refractive index change, $n_B - n_A$, as is the wavelength shift, $\lambda_B^* - \lambda_A^*$. Therefore, if the relationship between the refractive index and the peak potential is known at a certain wavelength, one can evaluate the refractive index in the vicinity of the nanoparticles from the peak potential measured at the wavelength.

Theoretical Sensitivities of the Potential-Scanning LSPR Sensor. Here we discuss the above-mentioned peak potential shift for the potential-scanning LSPR sensor quantitatively. The real part of the dielectric function of a metal (ε) is described by the simple Drude model. The damping parameter in the equation is often neglected[14,18,19] because it has little effect on the results obtained. Thus, the function is described as follows:[18,19]

$$\varepsilon = \varepsilon_\infty - \frac{{\omega_p}^2}{\omega^2} = \varepsilon_\infty - \frac{\lambda^2}{{\lambda_p}^2} \quad (1)$$

where ε_∞ is the high-frequency dielectric constant of the metal, ω is the frequency of light, and ω_p and λ_p are the bulk plasma frequency and wavelength, respectively, given by

$$\lambda_p = \frac{2\pi c}{\omega_p} = 2\pi c e\sqrt{\frac{m\varepsilon_0}{N}} \quad (2)$$

where c, e, m, ε_0, and N are the speed of light, the elementary charge, the electron mass, the vacuum permittivity, and the free electron density in the metal, respectively. Under the resonance condition of an uncoated and spherical metal nanoparticle (eq 3),[18]

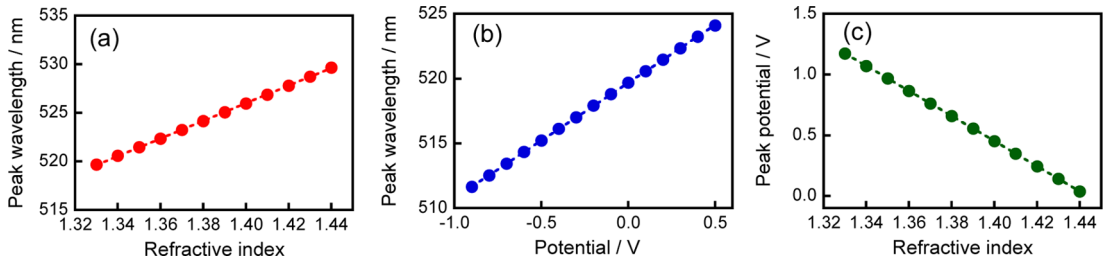

Figure 2. (a) Theoretical relationship between $\lambda^*_{E_0}$ and n, (b) that between λ^*_E and ΔE, and (c) that between E^*_λ and n (λ = 530 nm) for 13 nm Au nanoparticles.

eq 1 can be transformed to eq 4, showing the correlation between the LSPR wavelength at the rest potential E_0 ($\lambda^*_{E_0}$) and refractive index of the surrounding medium (n):

$$\varepsilon = -2n^2 \tag{3}$$

$$\lambda^*_{E_0} = \lambda_p\sqrt{2n^2+\varepsilon_\infty} \tag{4}$$

The relationship for Au nanoparticles (λ_p = 131 nm and ε_∞ = 12.2)[18] is shown in Figure 2a. The plot is almost linear in a practical range for aqueous systems ($1.33 \le n < 1.45$), and the theoretical refractive index sensitivity of the spherical Au nanoparticles of conventional LSPR sensors $S_{\lambda-n}$ is calculated to be ca. 95 nm RIU^{-1} (RIU = refractive index unit) from the slope of the approximate straight line for the plot.

On the other hand, the relationship between an applied potential $E = E_0 + \Delta E$ and the LSPR wavelength at E (λ^*_E) is given by the following equation:[13,16]

$$\frac{\lambda^{*2}_E}{\lambda^{*2}_{E_0}} - 1 = \frac{6CV\Delta E}{Fd} \tag{5}$$

where C, V, F, and d are the capacitance of the metal nanoparticle, the molar volume of the metal, the Faraday constant, and the diameter of the nanoparticle, respectively. Equations 4 and 5 give eq 6.

$$\lambda^*_E = \lambda_p\sqrt{(2n^2+\varepsilon_\infty)\left(\frac{6CV\Delta E}{Fd}+1\right)} \tag{6}$$

It was reported that the C value for citrate-capped Au nanoparticles with d = 3.7−40.8 nm is ca. 70 μF cm^{-2} at −0.4 to +0.6 V *vs* Ag|AgCl|saturated KCl.[16] The V value for Au is 10.2 cm^3 mol^{-1}. On the basis of these values, the relationship between λ^*_E and ΔE for Au nanoparticles with d = 13 nm in a solvent with n = 1.33 is drawn in Figure 2b. As can be seen from the figure, λ^*_E is almost linearly dependent on ΔE within the range of $-0.9 \le \Delta E \le +0.5$ V, and the theoretical potential sensitivity $S_{\lambda-E}$ under those conditions is determined to be ca. 8.9 nm V^{-1} from the slope of the approximate straight line.

At the potential to give the maximum extinction at a certain wavelength λ (peak potential E^*_λ), $\lambda = \lambda^*_E$ holds. Therefore, E^*_λ is described by eq 7, which is derived from eq 6.

$$E^*_\lambda = \frac{Fd}{6CV}\left(\frac{\lambda^2}{\lambda_p{}^2(2n^2+\varepsilon_\infty)}-1\right)+E_0 \tag{7}$$

The relationship between n and E^*_λ for 13 nm Au nanoparticles at λ = 530 nm is plotted on the basis of eq 7 in Figure 2c. The peak potential E^*_λ depends almost linearly on the refractive index n in the practical refractive index range, and the theoretical refractive index sensitivity S_{E-n} of the potential-scanning LSPR sensors with 13 nm Au nanoparticles is determined to be ca. 10.3 V RIU^{-1} from the negative slope of the approximate straight line.

If the sensitivities $S_{\lambda-n}$, $S_{\lambda-E}$, and S_{E-n} are constants, the following equation holds:

$$S_{E-n} = \frac{S_{\lambda-n}}{S_{\lambda-E}} \tag{8}$$

because $S_{E-n} = \Delta E^*_\lambda/\Delta n$, $S_{\lambda-n} = \Delta\lambda^*_E/\Delta n$, and $S_{\lambda-E} = \Delta\lambda^*_E/\Delta E^*_\lambda$. The S_{E-n} value estimated on the basis of eq 8 from the $S_{\lambda-n}$ and $S_{\lambda-E}$ values obtained from Figure 2a and Figure 2b, respectively, is 95/8.9 = 10.7, which is close to the S_{E-n} value obtained from Figure 2c (10.3). The small deviation suggests that the sensitivities are not completely constant. It is obvious from eq 8 that too large $S_{\lambda-E}$ could deteriorate the potential resolution. On the other hand, too small $S_{\lambda-E}$ could unduly broaden the potential scan range and give rise to undesirable oxidation or reduction reactions. In other words, the dynamic range of the sensor is limited when $S_{\lambda-E}$ is small. A moderate and appropriate $S_{\lambda-E}$ value is therefore required for a practical potential-scanning LSPR sensor.

Preparation of the Electrode. Electrodes modified with Au nanoparticles were prepared for demonstration of the potential-scanning LSPR sensing. Citrate-protected Au nanoparticles (13 nm diameter) were synthesized and electrostatically adsorbed onto an ITO electrode at pH 2.8, at which the ITO surface is positively charged[20] and citrate is negatively charged.[21] Figure 3a shows spectral changes during the adsorption. The extinction peak at ca. 530 nm is characteristic of absorption based on LSPR. The peak height was increased gradually and almost saturated in 120 min (Figure 3b). Therefore, the electrodes obtained by adsorption for 120 min were used for the following measurements. A typical scanning electron micrograph of the electrode surface

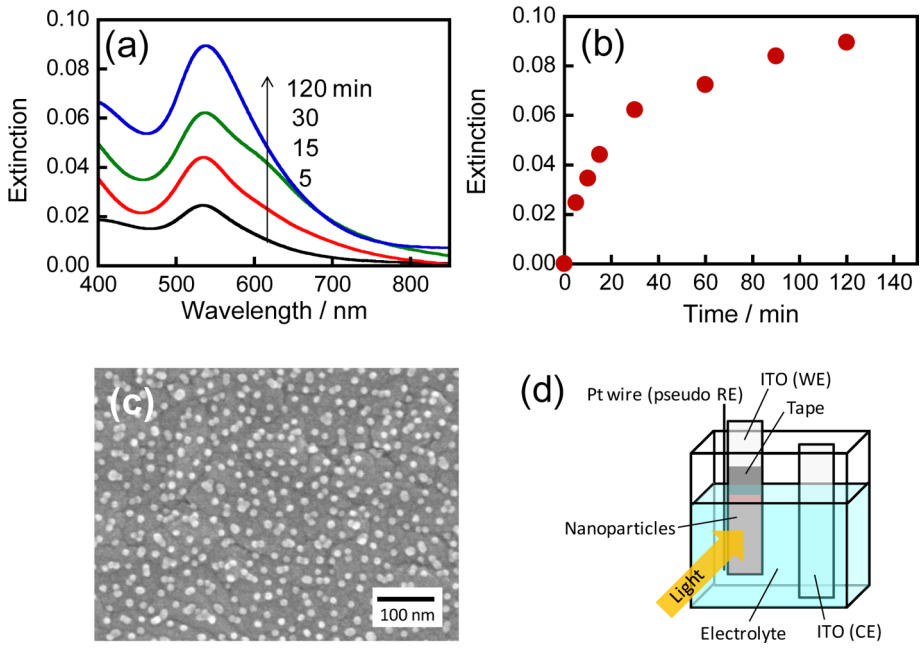

Figure 3. (a) Changes in the extinction spectrum of 13 nm Au nanoparticles adsorbed on an ITO electrode along with immersion of the electrode in an aqueous solution containing Au nanoparticles (pH = 2.8). (b) Time course of the extinction peak height in panel a. (c) Typical scanning electron micrograph of the electrode surface with the adsorbed Au nanoparticles. (d) Schematic illustration of the experimental setup for spetroelectrochemical measurements.

(Figure 3c) indicates that the Au nanoparticles are monodisperse and free from excess aggregation and agglomeration because of electrostatic repulsion between the negatively charged nanoparticles. These nanoparticles are therefore responsible for the relatively sharp peak, which is suitable for LSPR sensing. Au nanoparticles of 40 nm diameter were also adsorbed to the ITO surface successfully.

Sensitivity of Conventional LSPR Sensing. Figure 4a shows typical $\lambda-E-$ext and $\lambda-$ext plots for the ITO electrode modified with 13 nm Au nanoparticles in an aqueous solution containing 0.01 M KNO_3 (n = 1.333). The electrode showed the rest potential of ca. +0.3 V. The LSPR peak was red-shifted along with the positive potential scan as expected theoretically.[12−17] Typical $\lambda-E-$ext and $\lambda-$ext plots in aqueous solutions of sucrose (20, 30, and 50 wt %) containing 0.01 M KNO_3 are shown in Figure 4b−d. Refractive indices of the solutions were 1.364, 1.381, and 1.418, respectively. The peak wavelength shifted bathochromically with increasing refractive index of the solution. Actually, the plots of the peak wavelength at +0.12 to +0.42 V *vs* NHE as functions of the refractive index show positive slopes (Figure 5a). The error bars in the figure represent standard deviations of three or more independently fabricated electrodes. Refractive index sensitivity $S_{\lambda-n}$ at +0.12 to +0.42 V was evaluated from the slopes of the approximate straight lines in the figure to be 36 nm RIU^{-1}. The electrode modified with 40 nm Au nanoparticles was also examined in the same manner (Figure 6), and its $S_{\lambda-n}$ value was determined to be 44 nm RIU^{-1}.

Those values are smaller than the theoretical sensitivity calculated on the basis of eq 4 (95 nm RIU^{-1}). Protecting agents that cover the nanoparticles (*i.e.*, citrate molecules) are known to lower the sensitivity.[18] Actually, the refractive index sensitivity of Au nanoparticles with a diameter of 15 nm in a water−glycerol mixture was reported to be 44 nm RIU^{-1}.[4] The substrate on which the Au nanoparticles are deposited (*i.e.*, an ITO electrode) may also lower the sensitivity.[22] The sensitivity for Au nanoparticles with a diameter of 50 nm on a glass substrate was determined to be 60 nm RIU^{-1}.[23] The size dependence of the refractive index sensitivity is not described by eq 4 but by Mie theory, in which dipole and multipole plasmons are taken into account.[24] According to the calculation based on Mie theory,[24] it is expected that the sensitivity is increased by ∼1.2-fold, in good agreement with our experimentally observed dependence (44/36 = 1.2).

Potential Sensitivity. Figure 5b shows the relationships between the extinction peak wavelength and the applied potential for the electrode with 13 nm Au nanoparticles in solutions with different refractive indices. The slope of the plot, that is, potential sensitivity $S_{\lambda-E}$ of the electrode, is almost independent of the sucrose concentration (0−50 wt %) and is determined to be 8.3 nm V^{-1} from the slopes of the approximate straight lines in the figure. The experimentally evaluated potential sensitivity is in good accordance with the value expected theoretically from eq 6 (8.9 nm V^{-1}). In the case of the electrode with 40 nm Au nanoparticles, the potential sensitivity $S_{\lambda-E}$ was evaluated to be ca. 2.6 nm V^{-1}. This value is also close to the theoretically

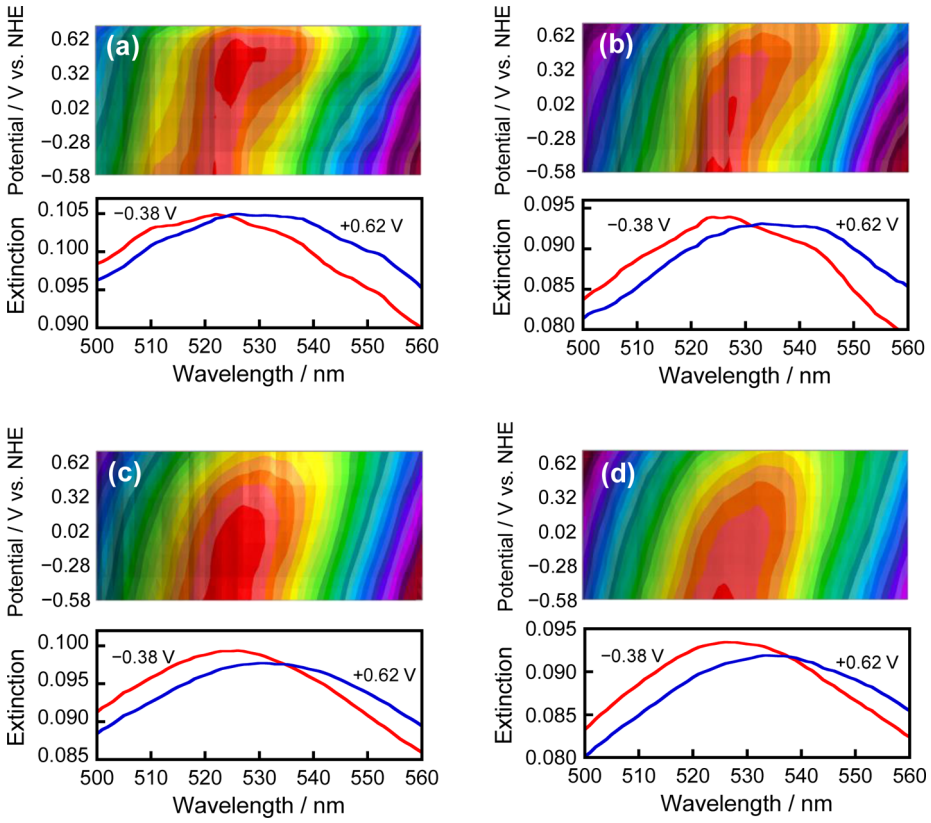

Figure 4. Typical $\lambda-E-$ext and $\lambda-$ext plots of 13 nm Au nanoparticle-modified ITO electrodes in (a) 0, (b) 20, (c) 30, and (d) 50 wt % aqueous sucrose solutions containing 0.01 M KNO_3. Potential range for the $\lambda-E-$ext plots is −0.58 to +0.72 V.

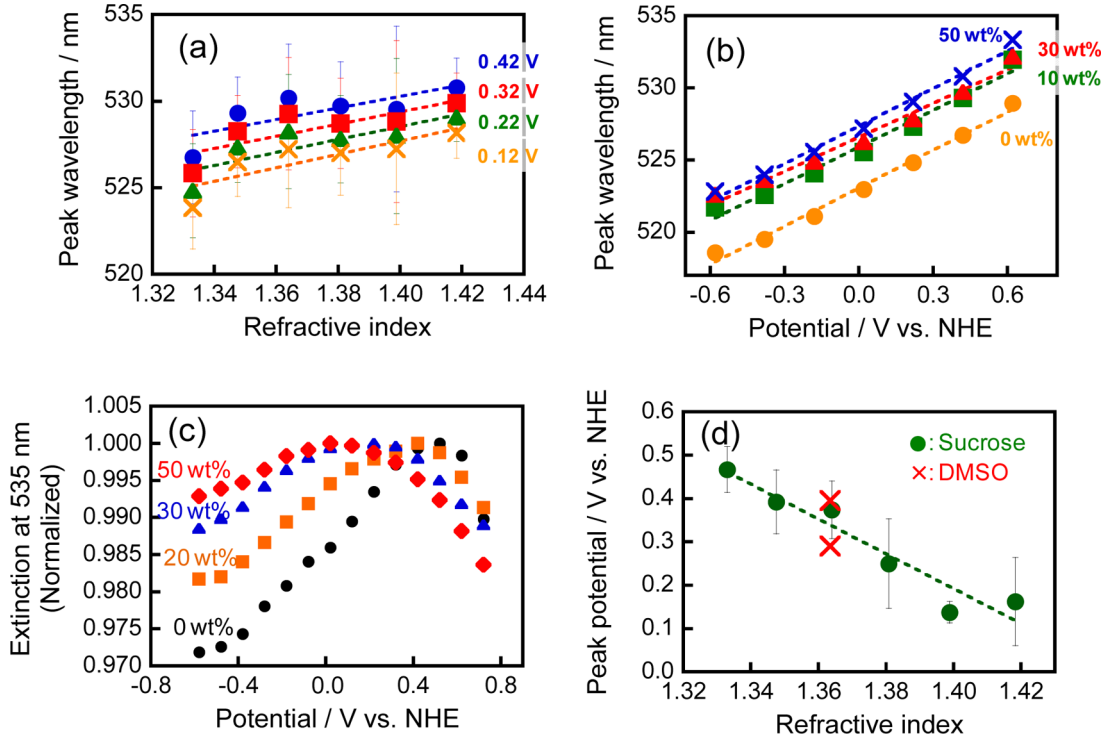

Figure 5. (a) Correlations between the refractive index n of the solution and the extinction peak wavelength λ_E^* at different applied potentials E for 13 nm Au nanoparticle-modified ITO electrodes. The solutions contain 0.01 M KNO_3. (b) Relationships between the applied potential E and the extinction peak wavelength λ_E^* at different sucrose concentrations (0−50 wt %). (c) Extinction−potential spectra at 535 nm in the sucrose solutions (0−50 wt %). (d) Relationship between the peak potential E_λ^* in panel c and the refractive index. The E_λ^* values in 20 vol % aqueous dimethylsulfoxide is also shown.

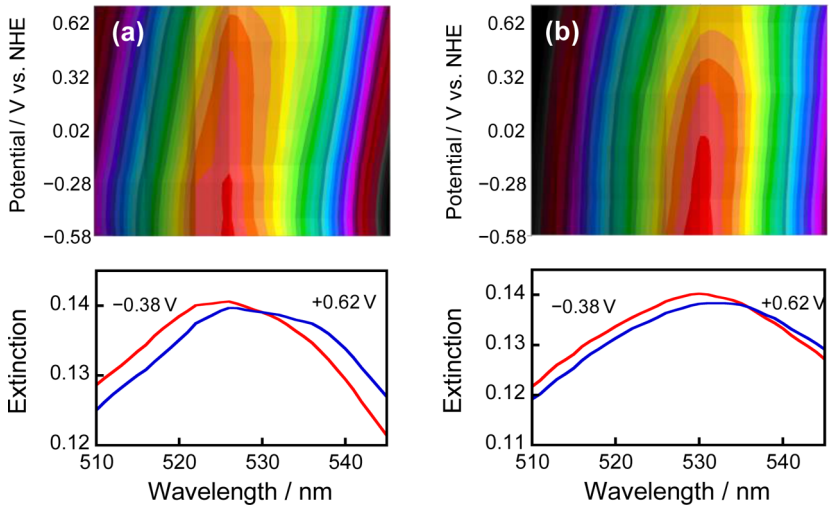

Figure 6. Typical $\lambda-E-$ext and $\lambda-$ext plots of 40 nm Au nanoparticle-modified ITO electrodes in (a) 20 and (b) 40 wt % aqueous sucrose solutions containing 0.01 M KNO_3. Potential range for the $\lambda-E-$ext plots is −0.58 to +0.72 V.

calculated value, 2.9 nm V^{-1}, which is lower than that of the electrode with 13 nm nanoparticles because of the larger d value in eq 6.

Sensitivity of Potential-Scanning LSPR Sensing. Figure 5c shows $E-$ext plots, namely, cross-sectional images of the $\lambda-E-$ext plots in Figure 4 at 535 nm, for 13 nm Au nanoparticles. As expected theoretically, peaks were obtained in the extinction−potential spectra, and the peak potential was shifted negatively with increasing refractive index of the solution. The relationship between the refractive index and the peak potential is shown in Figure 5d. The peak potentials were determined from the first derivatives of quartic equations fitted to the experimental data. The peak potential shows almost linear dependence on the refractive index of the solution, and the sensitivity S_{E-n} is determined to be ca. 4.0 V RIU^{-1} from the negative slope of the approximate straight line. The S_{E-n} value is in accordance with the value calculated from the experimentally obtained $S_{\lambda-n}$ and $S_{\lambda-E}$ values on the basis of eq 8 (36/8.3 = 4.3). Essentially, the same results were obtained even when sucrose was replaced with dimethylsulfoxide; the peak potentials appeared in the range that is predictable from the refractive index of the solution and Figure 5d. We therefore conclude that the potential-scanning LSPR sensor can be applied to different analytes.

In the case where 40 nm nanoparticles were used, the S_{E-n} value was about 16 V RIU^{-1}, in the range of $1.333 < n < 1.399$. This value is reasonable considering the $S_{\lambda-n}$ and $S_{\lambda-E}$ values (44/2.6 = 17). The higher sensitivity compared to that of the electrode with 13 nm particles is explained in terms of the larger $S_{\lambda-n}$ and smaller $S_{\lambda-E}$ values. High S_{E-n} gives rise to the high refractive index sensitivity but, simultaneously, the narrow dynamic range.

Thus, we have demonstrated that refractive index changes can be determined at a single wavelength by using the potential-scanning LSPR sensor proposed in this study. The smaller Au nanoparticles (13 nm diameter) give wider dynamic range, and the larger nanoparticles (40 nm) give higher refractive index sensitivity. The dynamic range may be broadened by covering the electrode surface with a thin layer of an electrochemically inactive and dielectric compound such as a metal oxide, which suppresses redox reactions even under higher overpotential applied.

We have reported that electrons transfer from a resonant plasmonic nanoparticle to an n-type semiconductor in contact with the nanoparticle on the basis of plasmon-induced charge separation (PICS),[25] which is recently known also as plasmonic hot electron injection. This effect would not interfere with the measurements in the present work because the efficiency of PICS is known to be low for a highly conductive semiconductor such as ITO.[26] Recently, it was also reported that electrons move between an illuminated plasmonic nanoparticle and ITO in direct contact so as to shift the peak wavelength toward the irradiation wavelength.[27] Although this effect might broaden the peak obtained by the potential scanning, it would be a few millivolts or less under weak illumination.

Improvement of Sensitivity of Potential-Scanning LSPR Sensing. In the previous section, easily preparable and commercially available spherical Au nanoparticles were used and the potential-scanning sensing was demonstrated by using those nanoparticles with moderate refractive index sensitivity. For fabrication of the sensor with high sensing capability, high $S_{\lambda-n}$ and moderate $S_{\lambda-E}$ are advantageous, as eq 8 indicates. It is known that the $S_{\lambda-n}$ value increases linearly with the LSPR peak wavelength,[4,28] which red shifts as, for instance, the particle shape anisotropy (*e.g.*, aspect ratio of nanorods) increases.[19] However, absorption of water gradually increases from 850 nm, so we use nanorods that are resonant at 700−800 nm (aspect ratio ∼3).

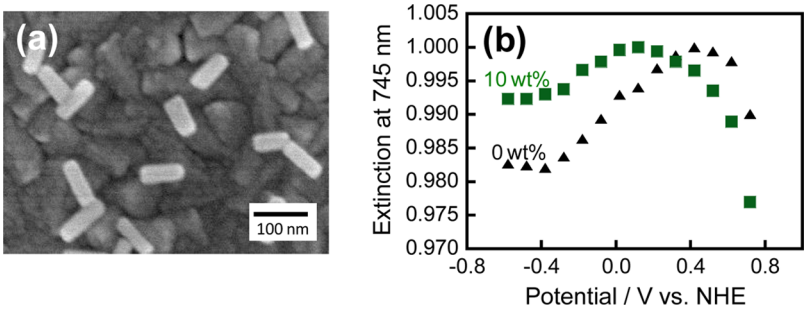

Figure 7. (a) Typical scanning electron micrograph of the electrode surface with the adsorbed Au nanorods. (b) Extinction−potential spectra for Au nanorod-modified ITO electrodes at 745 nm in the sucrose solutions (0 and 10 wt %) containing 0.01 M KNO_3.

According to the previously reported relationship between the peak wavelength and $S_{\lambda-n}$, the $S_{\lambda-n}$ value for Au nanoparticles resonant at 700−800 nm is estimated to be 340−500 nm RIU^{-1}, which is higher than those of the spherical nanoparticles used in the previous sections.

On the other hand, $S_{\lambda-E}$ is also dependent on the anisotropy of the particle shape. Mulvaney *et al.* reported that Au nanorods exhibit higher $S_{\lambda-E}$ than isotropic nanoparticles because the particle shape factor (L) affects the sensitivity of the LSPR peak wavelength to the free electron density N as follows.[29,30]

$$\lambda_E^* - \lambda_{E_0}^* = -\frac{N}{2N}\lambda_p\sqrt{\left(\frac{1-L}{L}\right)n^2 + \varepsilon_\infty} \qquad (9)$$

The L values for the Au nanosphere and nanorod with an aspect ratio of ca. 3 are 1/3 and 0.06−0.10, respectively.[31] Assuming that the relationship between ΔN and the applied potential is not dependent on the particle shape, the $S_{\lambda-E}$ value of the nanorod is expected to be 1.3−1.6 times higher than that of the nanosphere with the diameter corresponding to the nanorod width. Since the estimated increase in $S_{\lambda-n}$ is sufficiently higher than that in $S_{\lambda-E}$, significant improvement in the sensitivity S_{E-n} is expected for the potential scanning LSPR sensor.

Au nanorods were prepared according to a previous literature.[32] Figure 7a shows a typical scanning electron micrograph of the electrode surface with the adsorbed Au nanorods. Length, width, aspect ratio, and the extinction peak wavelength in water of the longitudinal mode are 80 ± 11 nm, 30 ± 8 nm, ca. 2.8, and 730 nm, respectively. Thus, the nanorods were synthesized successfully. The $S_{\lambda-n}$ value was evaluated from the extinction peak wavelengths in 0−20 wt % aqueous sucrose solutions to be 276 nm RIU^{-1}, which is about 7-fold higher than that for the spherical nanoparticles. The $S_{\lambda-E}$ value evaluated at −0.18 to +0.82 V *vs* NHE was ca. 12 nm V^{-1}, which is 1.4 and 4.6 times higher than 13 and 40 nm Au nanospheres, respectively. Figure 7b shows E−ext plots of the nanorod-modified electrode at 745 nm. As can be seen from the figure, the peak potential shifts largely as the sucrose content increases from 0 to 10 wt %. The S_{E-n} value is ca. 22 V RIU^{-1}, in good accordance with the value expected from eq 8 (276/12 = 23).

In order to evaluate the sensing capability of each nanoparticle, figure of merit (FOM), which is defined as the sensitivity divided by the full width at half-maximum (fwhm) of the peak, is often employed as a useful index. The fwhm value for the E−ext plot (ΔE_W) was evaluated by Lorentzian fitting around the peak top and the FOM of the present sensor ($S_{E-n}/\Delta E_W$) was calculated. The FOM values for the 13 and 40 nm Au nanospheres and the Au nanorod are ca. 0.4, 1.1, and 2.2, respectively. Thus, the sensing capability of the potential-scanning LSPR sensor was successfully improved by the use of the Au nanorods.

CONCLUSION

In this study, the principle of potential-scanning LSPR sensors as a new class of LSPR sensors was proposed and developed. We loaded an ITO electrode with Au nanospheres or nanorods and scanned its potential in an electrolyte solution to obtain an extinction−potential spectrum with an extinction peak. The peak potential shifted negatively with increasing refractive index of the solution, as expected theoretically. The linear peak shift would allow application of the electrode to chemical sensing or biosensing by modification of the nanoparticles with receptors selective to an analyte. Smaller nanoparticles should be selected for a wider dynamic range and larger ones for a higher sensitivity. The use of nanorods further improves the sensitivity and figure of merit.

METHODS

ITO electrodes loaded with Au nanoparticles were used as potential-scanning LSPR sensors. An aqueous solution (50 mL) of trisodium citrate (120 mg) was added quickly to a boiling aqueous solution (100 mL) containing tetrachloroaurate(III) tetrahydrate (40 mg), and the mixed solution was refluxed for 30 min to give an aqueous solution of Au nanoparticles with a mean diameter of 13 nm.[33] Au nanoparticles with a diameter of 40 nm were purchased from Tanaka Kikinzoku. A cleaned ITO electrode was immersed in a

nanoparticle solution with the pH adjusted to ca. 2.8 for 120 min.

Spectroelectrochemical measurements were carried out in an aqueous solution of sucrose (0−50 wt %) containing 0.01 M KNO_3 with the Au nanopaticle-modified ITO electrode (~2 cm^2), a platinum wire, and a bare ITO (~2 cm^2) as working, pseudo-reference, and counter electrodes, respectively (Figure 3d). The electrolyte concentration has little effect on the S_{E-n} value. The potential was scanned with a potentiostat (Princeton 263A) from −0.58 to +1.42 V and back to −0.58 V at 2 mV s^{-1}. The extinction spectrum of the electrode was obtained every 50 s (100 mV each) by an array spectrophotometer (Otsuka Electronics MCPD-3000) equipped with a light source (Otsuka Electronics MC-2530). We obtained $\lambda-E-$ext plots from the extinction spectra collected in the second positive scan from −0.58 to +0.72 V.

Conflict of Interest: The authors declare no competing financial interest.

Acknowledgment. This work was supported by a Grant-in-Aid for Young Scientists (B) (No. 26810043) and a Grant-in-Aid for Scientific Research (No. 25288063) from the Japan Society for the Promotion of Science.

REFERENCES AND NOTES

1. Willets, K. A.; Van Duyne, R. P. Localized Surface Plasmon Resonance Spectroscopy and Sensing. *Annu. Rev. Phys. Chem.* **2007**, *58*, 267–297.
2. Anker, J. N.; Hall, W. P.; Lyandres, O.; Shah, N. C.; Zhao, J.; Van Duyne, R. P. Biosensing with Plasmonic Nanosensors. *Nat. Mater.* **2008**, *7*, 442–453.
3. Stewart, M. E.; Anderton, C. R.; Thompson, L. B.; Maria, J.; Gray, S. K.; Rogers, J. A.; Nuzzo, R. G. Nanostructured Plasmonic Sensors. *Chem. Rev.* **2008**, *108*, 494–521.
4. Mayer, K. M.; Hafner, J. H. Localized Surface Plasmon Resonance Sensors. *Chem. Rev.* **2011**, *111*, 3828–3857.
5. Jain, P. K.; Huang, W.; El-Sayed, M. A. On the Universal Scaling Behavior of the Distance Decay of Plasmon Coupling in Metal Nanoparticles Pairs: A Plasmon Rule Equation. *Nano Lett.* **2007**, *7*, 2080–2088.
6. Mirkin, C. A.; Letsinger, R. L.; Mucic, R. C.; Storhoff, J. J. A DNA-Based Method for Rationally Assembling Nanoparticles into Macroscopic Materials. *Nature* **1996**, *382*, 607–609.
7. Kazuma, E.; Tatsuma, T. Localized Surface Resonance Sensors Based on Wavelength-Tunable Spectral Dip. *Nanoscale* **2014**, *6*, 2397–2405.
8. Svedendahl, M.; Chen, S.; Dmitriev, A.; Käll, M. Refractometric Sensing Using Propagating versus Localized Surface Plasmons: A Direct Comparison. *Nano Lett.* **2009**, *9*, 4428–4433.
9. Roh, S.; Chung, T.; Lee, B. Overview of the Characteristics of Micro- and Nano-structured Surface Plasmon Resonance Sensors. *Sensors* **2011**, *11*, 1565–1588.
10. Homola, J.; Yee, S. S.; Gauglitz, G. Surface Plasmon Resonance Sensors: Review. *Sens. Actuators, B* **1999**, *54*, 3–15.
11. Homola, J. Surface Plasmon Resonance Sensors for Detection of Chemical and Biological Species. *Chem. Rev.* **2008**, *108*, 462–493.
12. Ali, A. H.; Luther, R. J.; Foss, C. A., Jr. Optical Properties of Nanoscopic Gold Particles Adsorbed at Electrode Surfaces: The Effect of Applied Potential on Plasmon Resonance Absorption. *Nanostruct. Mater.* **1997**, *9*, 559–562.
13. Ung, T.; Giersig, M.; Dunstan, D.; Mulvaney, P. Spectroelectrochemistry of Colloidal Silver. *Langmuir* **1997**, *13*, 1773–1782.
14. Ali, A. H.; Foss, C. A., Jr. Electrochemistry Induced Shifts in the Plasmon Resonance Bands of Nanoscopic Gold Particles Adsorbed on Transparent Electrodes. *J. Electrochem. Soc.* **1999**, *146*, 628–636.
15. Toyota, A.; Nakashima, N.; Sagara, T. UV−Visible Transmission-Absorption Spectral Study of Au Nanoparticles on a Modified ITO Electrode at Constant Potentials and under Potential Modulation. *J. Electroanal. Chem.* **2004**, *565*, 335–342.
16. Toyota, A.; Sagara, T. Particle Size Dependence of the Charging of Au Nanoparticles Immobilized on a Modified ITO Electrode. *Electrochim. Acta* **2008**, *53*, 2553–2559.
17. Miyazaki, T.; Hasegawa, R.; Yamaguchi, H.; Oh-oka, H.; Nagato, H.; Amemiya, I.; Uchikoga, S. Electrochemical Control of Plasmon Resonance of Gold Nanoparticles Using Electrochemical Oxidation. *J. Phys. Chem. C* **2009**, *113*, 8484–8490.
18. Templeton, A. C.; Pietron, J. J.; Murray, R. W.; Mulvaney, P. Solvent Refractive Index and Core Charge Influence on the Surface Plasmon Absorbance of Alkanethiol Monolayer-Protected Gold Clusters. *J. Phys. Chem. B* **2000**, *104*, 564–570.
19. Chen, H.; Kou, X.; Yang, Z.; Ni, W.; Wang, J. Shape- and Size-Dependent Refractive index Sensitivity of Gold Nanoparticles. *Langmuir* **2008**, *24*, 5233–5237.
20. Daido, T.; Akaike, T. Electrochemistry of Cytochrome *c*: Influence of Coulombic Attraction with Indium Tin Oxide Electrode. *J. Electroanal. Chem.* **1993**, *334*, 91–106.
21. Alvarez-Puebla, R. A.; Arceo, E.; Goulet, P. J. G.; Garrido, J. J.; Aroca, R. F. Role of Nanoparticle Surface Charge in Surface-Enhanced Raman Scattering. *J. Phys. Chem. B* **2005**, *109*, 3787–3792.
22. Novo, C.; Funston, A. M.; Pastoriza-Santos, I.; Liz-Marzán, L. M.; Mulvaney, P. Influence of the Medium Refractive Index on the Optical Properties of Single Gold Triangular Prisms on a Substrate. *J. Phys. Chem. C* **2008**, *112*, 3–7.
23. Sun, Y.; Xia, Y. Increased Sensitivity of Surface Plasmon Resonance of Gold Nanoshells Compared to That of Gold Solid Colloids in Response to Environmental Changes. *Anal. Chem.* **2002**, *74*, 5297–5305.
24. Kvasnička, P.; Homola, J. Optical Sensors Based on Spectroscopy of Localized Surface Plasmons on Metallic Nanoparticles: Sensitivity Considerations. *Biointerphases* **2008**, *3*, FD4–FD11.
25. Tian, Y.; Tatsuma, T. Mechanisms and Applications of Plasmon-Induced Charge Separation at TiO_2 Films Loaded with Gold Nanoparticles. *J. Am. Chem. Soc.* **2005**, *127*, 7632–7637.
26. Kawahara, K.; Suzuki, K.; Ohko, Y.; Tatsuma, T. Electron Transport in Silver-Semiconductor Nanocomposite Films Exhibiting Multicolor Photochromism. *Phys. Chem. Chem. Phys.* **2005**, *7*, 3851–3855.
27. Sheldon, M. T.; van de Groep, J.; Brown, A. M.; Polman, A.; Atwater, H. A. Plasmoelectric Potentials in Metal Nanostructures. *Science* **2014**, *346*, 828–831.
28. Miller, M. M.; Lazarides, A. A. Sensitivity of Metal Nanoparticle Surface Plasmon Resonance to the Dielectric Environment. *J. Phys. Chem. B* **2005**, *109*, 21556–21565.
29. Mulvaney, P.; Pérez-Juste, J.; Giersig, M.; Liz-Marzán, L. M.; Pecharromán, C. Drastic Surface Plasmon Mode Shifts in Gold Nanorods Due to Electron Charging. *Plasmonics* **2006**, *1*, 61–66.
30. Novo, C.; Funston, A. M.; Gooding, A. K.; Mulvaney, P. Electrochemical Charging of Single Gold Nanorods. *J. Am. Chem. Soc.* **2009**, *131*, 14664–14666.
31. Prescott, S. W.; Mulvaney, P. Gold Nanorod Extinction Spectra. *J. Appl. Phys.* **2006**, *99*, 123504.
32. Ming, T.; Zhao, L.; Yang, Z.; Chen, H.; Sun, L.; Wang, J.; Yan, C. Strong Polarization Dependence of Plasmon-Enhanced Fluorescence on Single Gold Nanorods. *Nano Lett.* **2009**, *9*, 3896–3903.
33. Turkevich, J.; Stevenson, P. C.; Hillier, J. A Study of the Nucleation and Growth Processes in the Synthesis of Colloidal Gold. *Discuss. Faraday Soc.* **1951**, *11*, 55–75.